JOURNAL OF NATURAL PRODUCTS

ARTICLE

pubs.acs.org/jnp

Unraveling the Bastarane and Isobastarane Oximo Amide Configurations and Associated Macrocycle Conformations: Implications of Their Influence on Bioactivities

Wayne D. Inman* and Phillip Crews*

Department of Chemistry and Biochemistry, University of California, Santa Cruz, California 95064, United States

Supporting Information

ABSTRACT: Our rigorous re-examination of the conformational properties of bastadins that comprise the isobastarane and bastarane-type macrocycle has generated some interesting new insights. We determined that these macrocycles are flexible and possess a surprising degree of reflection symmetry that generates enantiomeric conformations. The macrocycle symmetry arises from its ability to twist in a disrotatory fashion, providing one set of conformers, and then twists with the opposite disrotation to generate a corresponding set of enantiomers. Overall, the isobastarane conformations for (*E*,*E*)-bastadin 19 (**1a**) are complex and can access several distinct ring conformations. In contrast, the bastarane macrocycle in bastadin 5 (**2**) and bastadin 6 (**3**) maintains a similar overall shape. We postulate that the short-term stability of the (*Z*)-oximo amide, an uncommon configuration found in bastadins and psammaplins, is due to the existence of conformers with intramolecular hydrogen bonds involving the (*Z*)-oxime, and hydrogen bonding impedes oxime isomerization to the more stable (*E*)-oximo amide in solution. Finally, the modeling results provided insights toward understanding the different antiproliferative activity against endothelial cells as well as Ca^{2+} channel modulation activities attributed to bastaranes **2** and **3** versus isobastarane **1a**.

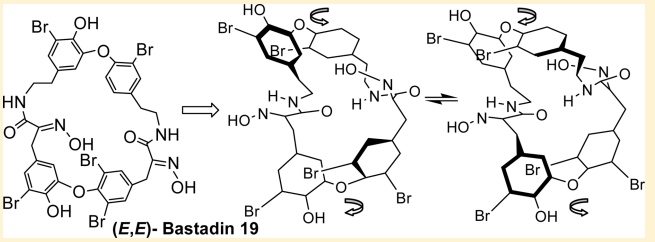

The oxime functional group, while an important organic chemistry synthon,[1] is uncommon in natural products. This moiety may exist as an *E* or *Z* diastereomer and undergoes acid-catalyzed or nucleophile-mediated isomerization in solution.[2] Natural products containing a (*Z*)-oxime, derived from tyrosine or *p*-phenylglycine and embedded in an 2-oximo amide or 2-oximo acid/ester moiety, are uncommon. Nocardicin A, a β-lactam including a (*Z*)-oximo amide, was isolated from the actinomycete *Nocardia uniformis* along with the minor *E* isomer, nocardicin B.[3,4] Nocardicins A and B were reported as a separable mixture and did not isomerize in solution. Conversely, psammaplins and bastadins are typically reported with the (*E*)-oximo amide configuration.[5−7] The 2-oximo acids and esters are exceptionally rare in nature. (*E*)-2-(Oximo)-3-phenylpropanoic acid and 2-(oximo)-3-(4-hydroxyphenyl)propanoic acid have been reported from marine sponges.[8,9] The fungal metabolite JBIR-25 was reported to contain exclusively the (*E*)-oximo ester,[10] contrary to what appears to be the identical compound assigned to aspergillusol A, reported simultaneously in the literature with the *Z* configuration.[11]

The factors responsible for the divergent patterns in the isolation of natural product containing (*Z*)-oximo amides or esters, as either a mixture or a single diastereomer, are not well understood. Over 20 years ago we reported (*Z*,*Z*)-psammaplin A,[5] whereas Schmitz observed the fleeting presence of (*E*,*Z*)-psammaplin A along with the *Z*,*Z* isomer from the same marine sponge.[6] Schmitz postulated "that either *E*,*Z* (or the *Z*,*Z* isomer

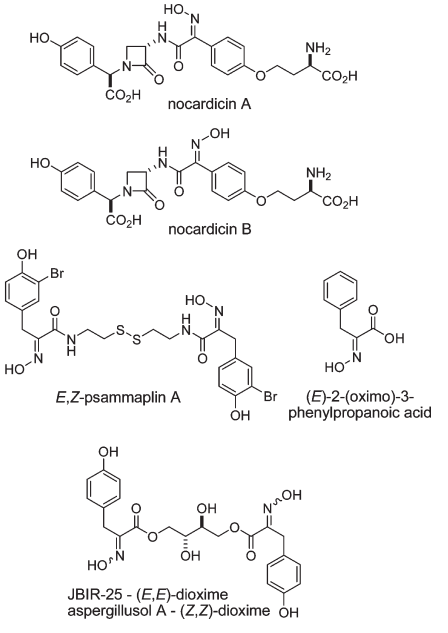

Special Issue: Special Issue in Honor of Koji Nakanishi

Received: November 3, 2010
Published: January 07, 2011

dx.doi.org/10.1021/np100798q | *J. Nat. Prod.* 2011, 74, 402–410

thereof) is the natural metabolite and that isomerization during extraction, extract storage, and/or chromatography results in *E,E* being isolated as the predominant product." Until recently, all bastadin metabolites have been reported with the (*E,E*)-dioxomo amide configuration. The single exception is represented in our recent description of the known (*E,E*)-bastadin 19 (**1a**), accompanied by (*E,Z*)-bastadin 19 (**1b**).[12] We were intrigued by the rare occurrence of the (*Z*)-oximo amide in psammaplins and bastadins especially given the numerous publications on these metabolites, whereas biosynthetic work on nocardicins revealed the oxime biosynthethic pathway proceeded *syn* to the amide, yielding a (*Z*)-oximo amide.[13,14] We determined the solution stability of the oximo amide isomers of bastadin 19, supported with molecular modeling studies of a hypothetical model compound, and proposed that bastadin and psammaplin metabolites are produced with the (*Z*)-oximo amide in a similar fashion to that in nocardicin A.[12] The (*Z*)-oxime subsequently isomerizes to the more thermodynamically stable *E* isomer in solution.

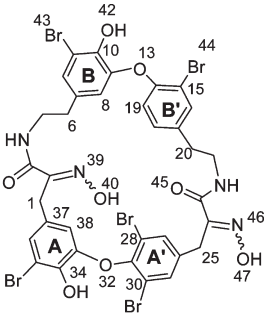

1a (*E,E*)-bastadin 19
1b (*E,Z*)-bastadin 19
1c (*Z,E*)-bastadin 19
1d (*Z,Z*)-bastadin 19

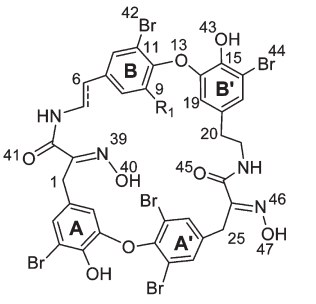

2 bastadin 5: R1 = H
3 bastadin 6: R1 = Br
4 bastadin 4: R1 = H, $\Delta^{5,6}$

Here we report on the molecular modeling studies on the intact bastadin macrocycle in order to understand the disparate observations reported for natural products containing (*Z*)- and/or (*E*)-oximo amides. Some details regarding the bastadins are important to review. The bastadins contain a 28-membered macrocycle that is commonly divided into either a bastarane or isobastarane based on the hydroxy-ether linkage in the northern bromocatechol bromophenyl ether. Bastadins 5 (**2**) and 6 (**3**) comprise the more common bastarane macrocycle, whereas bastadin 19 (**1a**−**d**), a constitutional isomer of bastadin 5, represents the isobastarane-type. Previous molecular modeling studies on **1a**, **2**, and **3** by Kobayashi reported the bastarane macrocycle was moderately rigid, whereas the isobastarane macrocycle was flexible.[15,16] By contrast, Molinski reported the macrocycle in **2** was flexible on the basis of NMR experiments.[17] Perplexed by these divergent views, we were inspired to further examine this phenomenon utilizing NMR and molecular modeling calculations. The results of this study support our previous hypothesis regarding the (*Z*)-oxime biosynthetic proposal. We now postulate that the short-term stability of the (*Z*)-oximo amide is due to the existence of conformers with an intramolecular hydrogen bond involving the (*Z*)-oxime, and hydrogen bonding impedes isomerization to the more stable (*E*)-oximo amide in solution. The conformational details gained from molecular modeling also provided insights on how the macrocycle conformation may affect antiproliferative activity against endothelial cells and as Ca^{2+} channel modulators.

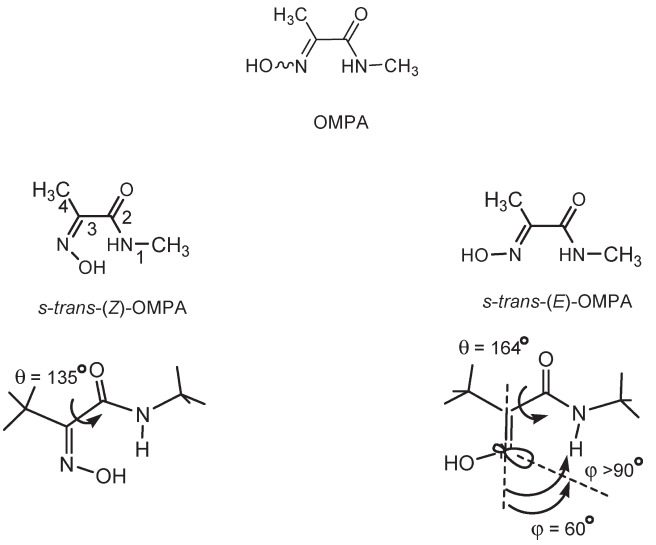

Figure 1. Calculated low-energy conformations for *s-trans*-(*Z*)-OMPA and *s-trans*-(*E*)-OMPA (lower images). The C═N bond is in the plane of the paper.

RESULTS AND DISCUSSION

The first step in this study involved rigorous conformational analysis through molecular modeling of the four bastadin 19 isomers consisting of (*E,E*)-bastadin 19 (**1a**), (*E,Z*)-bastadin 19 (**1b**), (*Z,E*)-bastadin 19 (**1c**), and (*Z,Z*)-bastadin 19 (**1d**). We utilized ^{1}H NMR data to calibrate the progress of the molecular mechanics and dynamics calculations. One goal was to assess if there was a stabilizing or steric interaction, perhaps from hydrogen bonding in the isobastarane macrocycle, that prolonged the lifetime of the (*Z*)-oximo amide moiety in **1b** while in solution. This isomer was stable for several weeks, even with a trace amount of formic acid present during the purification process. A second element of our design involved the modeling analysis of bastadin 5 (**2**) and bastadin 6 (**3**) to determine if there are any conformational differences between the two types of macrocycles that may explain the lack of any (*Z*)-oximo amide reported for the more common bastaranes.

Our previous report on the modeling results for the hypothetical compound (*E*)- and (*Z*)-2-(oximo)-*N*-methylpropanamide (OMPA), a simplified model for the oximo amide moiety found in bastadins, utilized the MMX force field.[12] We have now found that the MMX force field with the hydrogen bond term overestimates the contribution of hydrogen bonding.[18] In contrast, the MMFF94 force field provided an energy-minimized structure for *s-trans*-(*Z*)-OMPA (Figure 1) with bond lengths within the range reported in comparable crystal structures.[19] For example, the calculated N−O bond distance between amide N and oxime O was 2.69 Å, within the experimental range of 2.7−3.3 Å, along with a hydrogen bond between the amide H and oxime O with a distance of 2.04 Å. The dihedral angle $\theta_{N1-C2-C3-C4}$ was 135° due to a 45° twist from planarity caused by nonbonded interactions. A similar hydrogen bond was assigned to the (*Z*)-oximo amide in nocardicin A, on the basis of the amide ^{1}H NMR downfield shift of 0.3 ppm compared to the amide resonance in nocardicin B. Alternatively, no hydrogen bonding was detected in the (*E*)-oximo amide.[20,21] This was the distinction used to elucidate the oxime configuration in nocardicins A and B.

We believe there is no appreciable hydrogen bonding in *s-trans*-(*E*)-OMPA, in contrast to *s-trans*-(*Z*)-OMPA. As noted

dx.doi.org/10.1021/np100798q | *J. Nat. Prod.* 2011, 74, 402–410

Table 1. Relative Minimized Energies and Intramolecular Hydrogen Bond Types for (*E*,*E*)-Bastadin 19 (1a), (*E*,*Z*)-Bastadin 19 (1b), (*Z*,*E*)-Bastadin 19 (1c), and (*Z*,*Z*)-Bastadin 19 (1d) Conformers[a]

1a		1b		1c		1d	
relative energy (kJ/mol)	H-bond[b]	relative energy (kJ/mol)	H-bond[b]	relative energy (kJ/mol)	H-bond[b]	relative energy (kJ/mol)	H-bond[b]
0.0	1	0.0	1	0.0	1	0.0	1
1.1	1	1.5	1	0.3	1	1.0	1
1.2	2 + 3	2.3	2 + 3	6.2	4	3.6	1
3.0	3	5.8	1	7.2	1	7.2	1
4.8	3	6.3	1	7.5	3	7.9	3
6.6	2	7.8	2 + 3	7.9	1	8.4	2 + 3
7.1	2	8.3	2 + 3	8.4	none		
7.5	4	9.8	2	10.7	2		
7.5	1	9.9	4	10.8	2		
7.6	2 + 3	11.4	3				
8.9	2 + 3						
9.1	4						
9.8	1						

[a] The relative minimized energies for **1a**−**d** are 0, 6.5, 8.5, and 16.3 kJ/mol, respectively. [b] H-bond: **type-1**: O41---H-N22 (carbonyl O---H amide); **type-2**: O45---H-O40 (carbonyl O---H oxime); **type-3**: O42---H-O47 (phenol O---H oxime) and O13---H-O42 (diphenyl ether O---H phenol); and **type-4**: O41---H-O47 (carbonyl O---H oxime); **type 2 + 3** contains **type-2** and **type-3**.

above, this is similar to the lack of intramolecular hydrogen bonding reported in nocardicin B ((*E*)-oximo amide). Alternatively, Molinski interpreted the X-ray structure of **4** and proposed a rigid, planar five-membered ring with a strong intramolecular hydrogen bond between the amide *N*H and the oxime N.[22] However intermolecular *N*-H---*O*═C bonds in crystal structures have shown a distinct preference to form near the direction of the sp^2 nonbonded electron pair,[23,24] and we expect a similar preference would occur in a hydrogen bond for *N*-H---*N*═C. In *s-trans*-(*E*)-OMPA there is poor orbital overlap between amide H and the lone pair of the oxime N. The optimum angle for a hydrogen bond is $\varphi = 60°$ (see Figure 1); however, φ is predicted from modeling calculations to be slightly > 90°, and no significant hydrogen bond would be predicted. The higher calculated energy using the MMFF94 force field for *s-trans*-(*Z*)-OMPA versus *s-trans*-(*E*)-OMPA (11.9 kJ/mol relative energy difference) is in good agreement with our previously reported **1a**−**d** photo and thermal isomerization results.[12,25] Although the *Z* isomer is stabilized by a hydrogen bond, the dihedral angle $\theta_{N1-C2-C3-C4}$ must twist 45° from planarity between the π-bonds with loss of resonance energy due to nonbonded interactions (see Figure 1), which raise its energy relative to the *E* isomer.

We next examined the ^{1}H NMR chemical shifts and coupling constants of the methylene and amide protons for **1a**−**d** to determine if there was any intramolecular hydrogen bonding between two oximo amides and/or other functional groups within the macrocycle that would impart rigidity.[12] All chemical shifts for each methylene were isochronous, indicative of a flexible macrocyle. Vicinal coupling constants for H_2-5/H_2-6 and H_2-20/H_2-21 displayed an A_2X_2 spin system with averaged coupling constants (6−7 Hz), representative of a rapid dynamic interconversion between two or more *gauche* rotamers. If the macrocycle were rigid, then the vicinal protons would display an ABXY spin system with divergent coupling constant values.

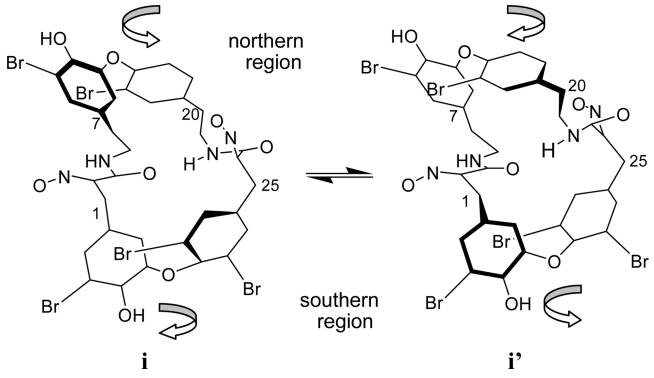

Figure 2. Illustrations of the two global energy minima conformers (**i** and **i**′ enantiomers) of (*E*,*E*)-bastadin-19 (**1a**). The overall disrotatory twisting motion of the macrocycle that generates each conformation is shown above and below the hydroxybromodiphenyl ether (HBDE) moieties. The orientation of each conformer is similar to the image shown on the left in Figure 3.

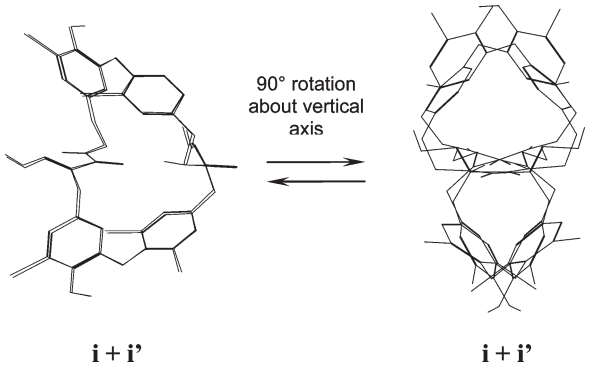

Figure 3. Superimposed views of the two global energy minima conformers (**i** + **i**′ enantiomers) of (*E*,*E*)-bastadin-19 (**1a**). To correlate the atom numbering with structural elements, see Figure 2. A 90° clockwise rotation about a vertical axis of the superimposed view of **i** + **i**′ on the left generates the superimposed view on the right and demonstrates the reflection symmetry of the enantiomers.

The conformational search for **1a**, **1b**, **1c**, and **1d** resulted in 13, 10, 9, and 6 unique diastereomeric conformations, respectively, predicted within a cutoff of 12 kJ/mol of the global minimum for each structure (see Table 1). Surprisingly, each individual conformer for **1a**−**d** possessed an enantiomeric form. Graphic illustrations of two global energy minima enantiomeric conformations (**i** and **i**′) for **1a** are shown in Figure 2 along with the direction of the disrotatory twisting motion with respect to the northern and southern regions of the macrocycle that leads to each conformation. The macrocycle symmetry arises from its ability to twist in a disrotatory fashion, providing one set of conformers, and then to twist with the opposite disrotation to generate a corresponding set of enantiomers. The perspectives of the superimposed imposition of the two global energy minima enantiomeric conformers (**i** + **i**′) for **1a** are shown in Figure 3. We call this conformational equilibrium between enantiomers "the bastadin dance"! The superimposed view of the 13 conformers for **1a** (Table 1) along with the description of the macrocycle twist direction that characterizes that diastereomeric set is depicted in Figure 4.

An analysis of each conformer for **1a**−**d** predicted that each conformer contains one or more intramolecular hydrogen bonds.

dx.doi.org/10.1021/np100798q | *J. Nat. Prod.* 2011, 74, 402–410

They are described in Table 1, and their relative contributions to the ensemble vary as a function of the oximo amide configuration. The different hydrogen bonds are coded in Figure 5 as **type-1**: O41---H-N22 (carbonyl O---H amide); **type-2**: O45---H-O40 (carbonyl O---H oxime); **type-3**: O42---H-O47 (phenol O---H oxime) and O13 ---H-O42 (diphenyl ether O---H phenol); and **type-4**: O41---H-O47 (carbonyl O---H oxime); as well as **types-2**+**3**, which is a combination of **type-2** and **type-3**.

The five categories of intramolecular hydrogen bonding shown in Figure 5 were used to characterize subsets of the 13 conformers of **1a** and defined the general shape of their ring conformations. In H-bond **type-1** there is a *trans*-annular hydrogen bond between carbonyl O41 and amide H-N22. Four conformers contain H-bond **type-1** and display a small degree of flexibility between two *gauche* rotamers at C5−C6 in addition to 180° rotations of the monobromophenyl ring B′. Alternatively, there are two conformers possessing a *trans*-annular hydrogen bond between carbonyl O45 carbonyl and oxime H-O40, denoted as H-bond **type-2**, which differs by an out of plane torsion about C2−C3. Another two conformers have H-bond **type-3**, consisting of two hydrogen bonds, one between phenol O42 and oxime H-O47 and the second between phenyl ether O13 and the phenol H-O42. Flexibility in this set involves torsion about oximo amide at C2−C3−N4. Three conformers have H-bond **types-2**+**3**, and flexibility in this set involves *gauche* rotamers about the C5−C6 and C20−C21. Finally, there were two conformers that contained a hydrogen bond from carbonyl O41 to oxime H at O47, denoted as H-bond **type-4**. The macrocycle flexibility in this case was due to ∼180° rotation of monobromophenyl ether in ring B′.

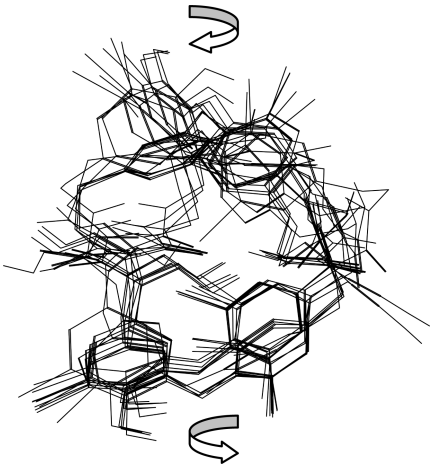

Figure 4. Superimposed view of the 13 conformers for (*E*,*E*)-bastadin-19 (**1a**). The overall disrotatory twisting motion of the macrocycle that generates the unique set of diastereomeric conformations is shown above and below the hydroxybromodiphenyl ether (HBDE) moieties. The superimposed view illustrates the greater degree of flexibility in the northern region of the macrocycle as compared to the southern region.

A previous modeling study of **1a** predicted the macrocycle to be flexible.[15] However, we believe the degree of flexibility was underestimated, as the enantiomeric relationship of the conformers was not found, nor was the diversity of hydrogen bonding types identified. The modeling results for **1a** presented in this study, supported in part by the ^{1}H NMR data, signify that the isobastarane macrocycle is very flexible. Isobastarane **1a** is capable of equilibrating between a total of 26 conformers, comprised of 13 diastereomers that have the same disrotational twist within the macrocycle and another 13 that are the enantiomers of the first set. Overall, there is considerable flexibility in the northern region containing the B/B′ aryl rings, as shown in Figures 4 and 5. Thus, the northern 2′-hydroxy-2,3′-dibromodiphenyl ether (HBDE)

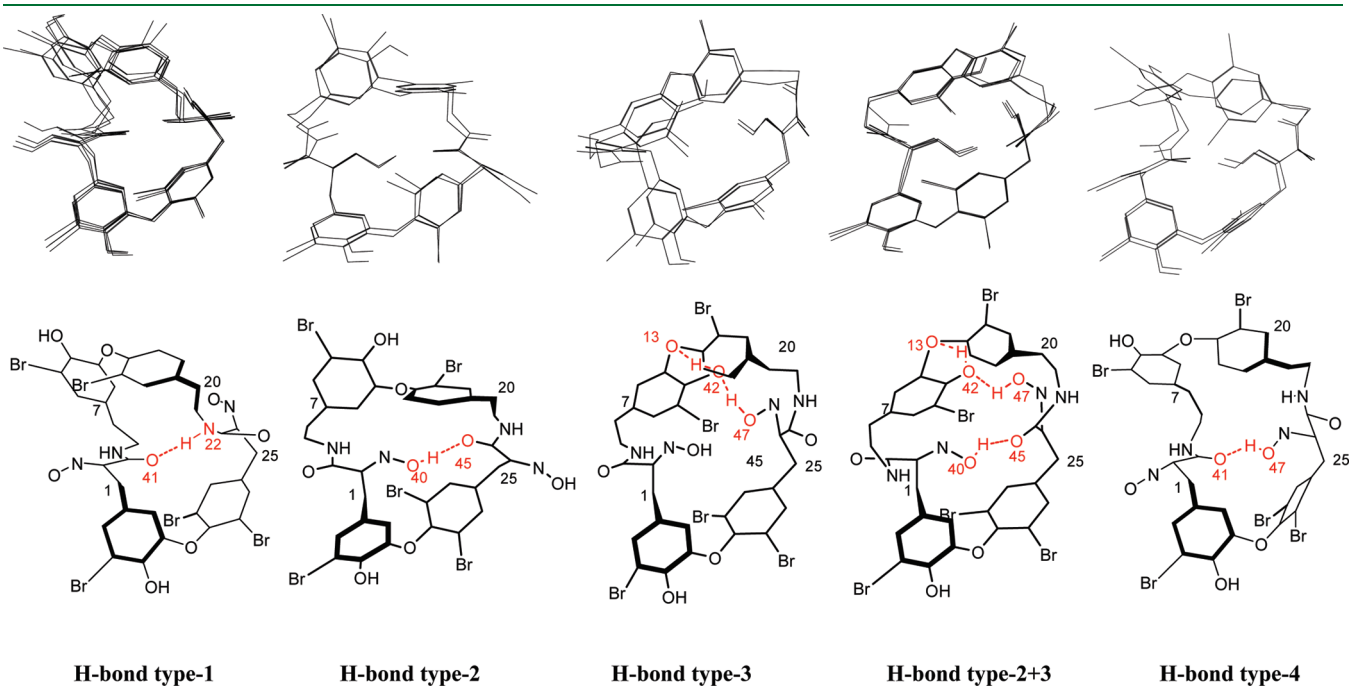

Figure 5. Superimposed views (top images) and graphic illustrations (bottom images) of each subset of conformations for (*E*,*E*)-bastadin-19 (**1a**); see Table 1. Each subset is based on a unique intramolecular hydrogen bond shown above. H-bond: **type-1**: O41---H-N22 (carbonyl O−H amide); **type-2**: O45---H-O40 (carbonyl O−H oxime); **type-3**: O42---H-O47 (phenol O−H oxime) and O13---H-O42 (diphenyl ether O---H phenol); **type-4**: O41---H-O47 (carbonyl O−H oxime); **type-2**+**3**: a combination of **type-2** and **type-3**.

dx.doi.org/10.1021/np100798q |*J. Nat. Prod.* 2011, 74, 402–410

Table 2. Dihedral Angles Defining the Diphenyl Ether Ring Orientation in (*E*,*E*)-Bastadin 19 (1a) and Bastadin 5 (2) Conformers[a]

	(*E*,*E*)-Bastadin-19 (**1a**)			
conformer relative E	$\theta_{28(30)-29-32-33}$	$\theta_{29-32-33-34(38)}$	$\theta_{10(8)-9-13-14}$	$\theta_{9-13-14-15(19)}$
0.0	−101.2	−162.8	−164.8	−97.6
1.1	−100.6	−162.3	−142.4	−113.1
1.2	−102.4	−162.5	−102.0	−130.0
3.0	−84.9	−160.4	−111.2	−159.2
4.8	−110.2	−157.7	−106.4	−128.5
6.6	−102.1	−166.8	−94.6	−155.7
7.1	−104.3	−165.9	−86.2	−168.3
7.5	−104.0	−160.5	142.9	−60.7
7.5	−98.2	−166.2	−176.6	−85.4
7.6	−102.7	−156.2	−94.6	−130.9
8.9	−102.7	−159.3	−94.4	−131.8
9.1	−101.0	−165.5	−130.3	−138.8
9.8	−99.3	−159.8	−170.8	−94.4
	Bastadin-5 (**2**)			
conformer relative *E*	$\theta_{28(30)-29-32-33}$	$\theta_{29-32-33-34(38)}$	$\theta_{9(11)-10-13-14}$	$\theta_{10-13-14-15(19)}$
0.0	−99.3	−161.9	−62.5	141.8
3.6	−102.5	−158.2	−53.1	147.1
3.9	−108.0	−156.5	−62.1	148.9
7.0	−100.3	−156.8	−67.4	139.8
7.1	−100.7	−160.5	−81.0	150.9
7.2	−97.7	−160.7	−100.7	−168.6
8.7	−103.5	−159.5	−47.5	130.3
8.9	−103.5	−159.8	−53.7	140.1
10.1	−99.4	−160.9	−79.8	146.0
10.4	−104.4	−157.6	−118.3	−144.0
10.8	−99.5	−157.4	−127.3	−140.0
11.7	−98.8	−166.4	−127.3	−138.6

[a] A combination of ±180° or ±90° for a pair of dihedrals within a HBDE (hydroxy bromodiphenyl ether) would represent two orthogonal rings.

adopts different conformations with respect to the macrocycle as well as a wide range of dihedral angles ($\theta_{10(8)-9-13-14}$ and $\theta_{9-13-14-15(19)}$) defining the relationship between the two phenyl rings B and B′ (see Table 2). By contrast, there is much less variance in dihedral angles ($\theta_{28(30)-29-32-33}$ and $\theta_{29-32-33-34(38)}$) representing the southern HBDE phenyl rings A and A′. In summary, the superimposed view of the 13 **1a** conformations in Figure 4 illustrates this differential flexibility in the northern versus southern regions of the isobastarane.

Similar modeling results were obtained for **1b**−**d** to those of **1a**, and the global minimum energy conformer for the latter was calculated to be the lowest energy of the set. Thus, the relative predicted stability order for this series is **1a** < **1b** < **1c** < **1d**, based on the relative energies for the global minima of 0, 6.5, 8.9, and 16.3 kJ/mol, respectively (Table 1). The calculated pattern agrees with our previous solution stability results, where **1b**−**d** isomerized to **1a**.[12] Interestingly, while the absolute number of low-energy minima within the 12 kJ/mol cutoff decreases in **1a**−**d** as the number of *Z* isomers increases, all exhibit intramolecular hydrogen bonding as defined in Table 1. We believe the key to short-term stability of the (*Z*)-oximo amide is due to the existence of higher energy conformers with intramolecular hydrogen bonds involving the (*Z*)-oxime, and hydrogen bonding impedes oxime isomerization to form the lowest energy diastereomer **1a** in solution. A mechanism illustrating acid-promoted *E*/*Z* oxime isomerization in water[2] is shown in Figure 6 and illustrates the process of transforming **1b** to **1a** by disruption of H-bond **type-3**. This specific conformation for **1b** contains H-bond **types-2**+**3** (see entry in Table 1) and is calculated to be 2.3 kJ/mol above the **1b** global minimum (and overall 8.8 kJ/mol above **1a** global minimum). In this case, the hydrogen bond (O42---H-O47) impedes C−N bond rotation to form (*E*)-oxime and returns the protonated oxime-water adduct to the starting (*Z*)-oxime. Otherwise, the hydrogen bond must be severed in the isomerization process.

Extension of this analysis to hydrogen-bonded (*Z*)-oximes in **1c** and **1d** revealed only conformers with substantially higher minimized energies (>8 kJ/mol above the global minimum) that would not exist to any appreciable degree in solution.[26] In **1c**, two conformers have a hydrogen-bonded (*Z*)-2-oxime and were calculated to be 10.7 and 10.8 kJ/mol above the **1c** global minimum. Similarly, in **1d**, two conformers with hydrogen bonds to (*Z*,*Z*)-2,24-dioximes were calculated to be 7.9 and 8.4 kJ/mol above the **1d** global minimum. The high calculated energies for these (*Z*)-oxime hydrogen-bonded conformers in **1c** and **1d** indicate they would not exist at any appreciable concentration in solution, and the remaining (*Z*)-oxime conformers have no hydrogen bonding and should readily isomerize to **1a**. This scenario corresponds to our inability to detect **1c** and **1d** during the isolation of **1a** and **1b**.

Modeling results obtained with **1a**−**d** provided an important perspective to re-examine psammaplin A and the feasibility of obtaining diastereomeric mixtures consisting of (*E*,*E*)-, (*E*,*Z*)-, and (*Z*,*Z*)-dioximo amides. We hypothesized that hydrogen bonding may contribute to prolong the lifetime of the *E*,*Z* diastereomer. Therefore, molecular modeling studies with (*E*,*Z*)-psammaplin A were undertaken to explore this point. A set of global and local minima contained an intramolecular hydrogen bond between the hydrogen of the (*Z*)-oxime and the phenol oxygen at the opposing end of the dimer (see Figure S1, Supporting Information), a new twist akin to hydrogen bond **type-3** in the bastadins. In this case, the acyclic chain of the conformers could interconvert between

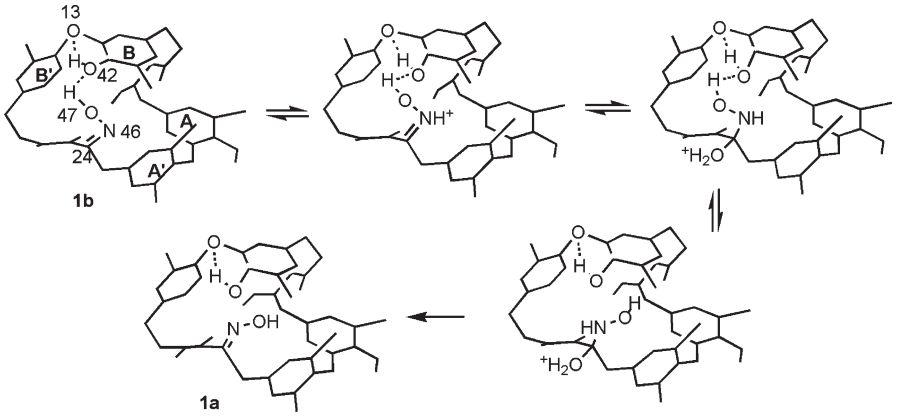

Figure 6. Proposed mechanism for (*Z*)- to (*E*)-oxime isomerization for **1b** to **1a** under acidic aqueous conditions[2] where intramolecular hydrogen bonding H-bond **type-3** impedes isomerization.

Table 3. Relative Minimized Energies and Intramolecular Hydrogen Bond Types for Bastadin 5 (2), Bastadin 6 (3), and Bastadin 4 (4) Conformers

2		3		4	
relative energy (kJ/mol)	H-bond[a]	relative energy (kJ/mol)	H-bond[a]	relative energy (kJ/mol)	H-bond[a]
0.0	2	0.0	2	0.0	none
3.6	2	2.2	2	1.2	none
3.9	2	4.6	2	2.7	none
7.0	2	4.6	2	5.6	none
7.1	2	6.1	2	6.1	none
7.2	2	7.8	2	7.7	none
8.7	2	8.8	2	8.1	none
8.9	2	11.0	1	11.5	4
10.1	2				
10.4	2				
10.8	2				
11.7	1				

[a] H-bond: **type-1**: O41---H-N22 (carbonyl O---H amide); **type-2**: O45---H-O40 (carbonyl O---H oxime); **type-4**: O41---H-O47 (carbonyl O---H oxime).

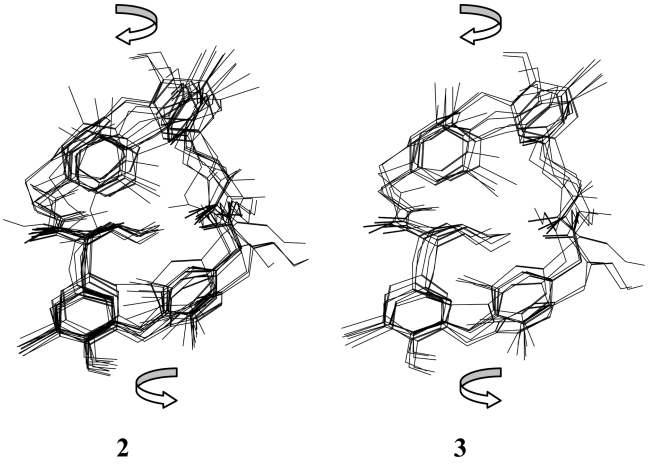

Figure 7. Superimposed view of the 12 conformers of bastadin 5 (**2**) and eight conformers of bastadin 6 (**3**); see Table 3. The overall disrotatory twisting motion of the macrocycle that generates these sets of unique diastereomeric conformations is shown above and below the hydroxybromodiphenyl ether (HBDE) moieties.

right-handed or left-handed helices. Our calculations were also consistent with the ^{1}H NMR coupling constants, revealing the acyclic chain was flexible in solution.[7] Thus, in a similar fashion to that discussed for **1**, the transitory hydrogen bond in the psammaplin A (*Z*)-oxime should prolong its lifetime in solution.

No (*Z*)-oximes have been reported to date for the bastarane-type macrocycles represented by **2**−**4**. The ^{1}H NMR coupling constant analysis and modeling results for **2** and **3** also indicate these macrocycles are conformationally mobile. The macrocycle in 5-[^{2}H]-**2** was reported to be flexible, and the spin system for H-5/H_2-6 displayed an A_2X system from room temperature to −50 °C.[17] Likewise, **3** must be flexible, as a similar A_2X_2 system was also reported.[27] Our modeling results for **2** and **3** predict the bastarane macrocycle to be flexible. Summarized in Table 3 are the 12 and 8 unique diastereomeric conformers predicted within a 12 kJ/mol cutoff for **2** and **3**, respectively. Also, as in the isobastarane case, each conformer can exist as a pair of enantiomers, and superimposed views of a unique set of diastereomeric conformers having the same disrotatory twist direction in the macrocycle are shown in Figure 7. Both **2** and **3** occupy a similar conformational space, and there are fewer conformations for **3** due to the symmetrical dibromophenyl B ring.

Additional observations based on the modeling results for **2** and **3** are the following. (a) The majority of conformers possess H-bond **type-2** (O45---H-O40), which characterizes the general shape of the macrocycle for **2** and **3**. (b) Conformational flexibility occurs mostly in the northern region of the macrocycle, including rotamers about C5−C6 and C20−C21, as well as flexibility about the oximo amide at N22−C23−C24. The dihedral angles defining the relationship between the diphenyl ether rings in the southern and northern HBDEs of **2** and **3** are shown in Table 2. In comparison to **1a**, the southern angles ($\theta_{28(30)-29-32-33}$ and $\theta_{29-32-33-34(38)}$) have similar values and the northern angles ($\theta_{9(11)-10-13-14}$ and $\theta_{10-13-14-15(19)}$) do not vary as widely. (c) Overall, our modeling results for **2** and **3** are counter to a previous modeling study concluding that these bastaranes were moderately rigid.[15,16] (d) H-bond **type-3** is not possible in bastaranes due to the alternate phenyl ether linkage and absence of the hydroxy group in the aromatic B ring and suggests why no (*Z*)-24-oximes have been reported within this more abundant class of bastadins. (e) We found no low-energy conformers with the (*Z*)-2-oxime configuration versus that of *E* in **2** or **3**. Thus, building upon the conclusions for **1**, we now propose that in the bastarane series, the initial (*Z*)-oxime

dx.doi.org/10.1021/np100798q | *J. Nat. Prod.* 2011, 74, 402–410

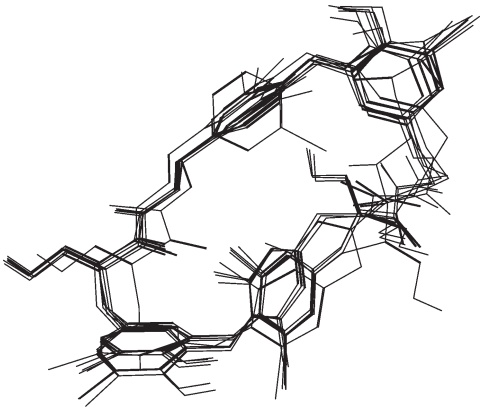

Figure 8. Superimposed view of the eight conformers of bastadin 4 (**4**).

biosynthetic product rapidly isomerizes to the more thermodynamically stable *E* isomer because no intramolecular hydrogen bond exists to impede the isomerization.

A final element of our study involved using the conformational properties described above to gain further insights into the biological activities of these structures. The potent and selective antiproliferative activity of **2** and **3** against human umbilical vein endothelial cells (HUVEC) was partially attributed to the conformational rigidity in the bastarane macrocycle, whereas only moderate activity was observed for **1a** along with a more flexible macrocycle.[15] Although our results indicate both bastarane and isobastarane macrocycles are flexible, we carried out the conformational analysis of bastadin 4 (**4**) to determine if similar conformational properties exist between **2**, **3**, and **4**, as all three have comparable antiproliferative activity. Starting with the crystal structure atom coordinates,[27] the modeling results indicated this macrocycle has a more restricted conformational space due to the *trans* double bond that effectively locked C2−C3−N4−C5−C6 into a planar group, consistent with the reported ^{1}H NMR coupling constant $^3J_{N4-H5}$ = 10.2 Hz,[27] requiring a dihedral angle of approximately 180°.[28] The minimized energies from the conformational search are listed in Table 3, and once again the conformers are enantiomeric. The superimposed view of one set of diastereomers is shown in Figure 8 and illustrates the elongated macrocycle due to the C2−C3−N4−C5−C6 planarity. The majority of conformers have no intramolecular hydrogen bond and do not resemble the macrocycle conformation for **2** and **3**. Given such substantial differences between the bastarane conformations **2** and **3** compared to **4** yet their similar activities, it is unlikely the overall macrocycle shape found in **2** and **3** is the defining feature for antiproliferative activity against HUVEC.

The bastadins have also displayed potent ryanodine receptor-1 (RyR1) calcium channel activity. Bastadins **2** and **3** bind to the RyR1-Ca^{2+} channel (EC_{50} 2.2, 2.6 μM, respectively), whereas **1a** is a weak partial agonist (EC_{50} >100 μM).[17,29] The contrasting activities between **1a** and **2** may be due to the different conformational aspects of the isobastarane versus bastarane macrocycle and their ability to bind to the receptor and affect channel function.[29] Although the isobastarane macrocycle in **1a** exhibits a mix of different conformations and H-bond types in comparison to bastarane **2**, **1a** was found to access a similar conformational space found in **2** and **3** as defined by H-bond **type-2**. The superimposed view of the three lowest energy conformers of **2** with **1a** conformers with H-bond **type-2**+**3** are shown in Figure 9 and indicates the overall macrocycle shapes are similar between

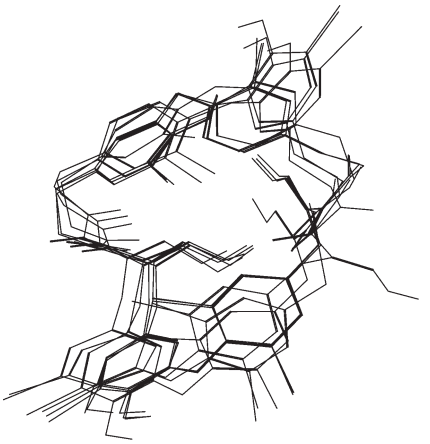

Figure 9. Superimposed view of the three lowest energy conformers for bastadin 5 (**2**) with conformers of (*E*,*E*)-bastadin 19 (**1a**) with H-bond **type-2**+**3**. The superimposed view indicates the overall macrocycle shapes are similar; however the bastarane and isobastarane macrocycles constrain the northern HBDE in an opposite configuration.

each bastadin type. Although all three can be similar in overall shape, the isobastarane macrocycle constrains the northern HBDE in an opposite configuration of that found in the bastaranes. Noteworthy differences between **2** and **1a** are observed in the northern HBDE. Specifically, the bromo and hydroxy groups are opposed in the B′ rings, and there is an *ortho*-bromo substituent at C-16 in **2**, but this position is unsubstituted in **1a**. This different configurational position of atoms in **1a** along with the constraints imposed by the macrocycle may not be optimal for binding or channel function.

Additional bastadin SAR studies have revealed details toward defining the minimum bastadin pharmaphore for the RyR-Ca^{2+} channel. The 2-bromo in HBDE is necessary for activity, whereas the oxime functional group is not.[29] Constraint of the diaryl ether moiety by the macrocycle is not a condition for activity; an acyclic HBDE-oxime analogue resembling the A,A′ diphenyl ether stimulated Ca^{2+} release via RyR2 (the major brain isoform).[30] Recently, hydroxylated metabolites of polybrominated diphenyl ethers (BDEs), commonly used as flame retardants and which pose a neurotoxicological risk, were reported to release Ca^{2+} from intracellular stores in PC12 cells at much lower concentrations than the corresponding parent congeners.[31,32] A limited SAR on several hydroxylated BDEs revealed the hydroxy-BDE **5** was more potent than analogues with an additional *ortho* substitution around the hydroxy group such as the HBDE substitution pattern found in the bastadins. A known BDE (**6**), commonly found in marine sponges of the genus *Dysidea*, was recently isolated from a red alga and found to increase intracellular Ca^{2+} in mouse neocortical neurons where the source of elevated Ca^{2+} was exclusively extracellular.[33] The elevated Ca^{2+} from extracellular stores may be due to the dissimilar cell line used in this case or from different actions by distinct BDEs.

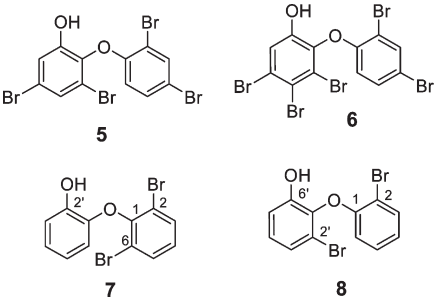

dx.doi.org/10.1021/np100798q |*J. Nat. Prod.* 2011, 74, 402–410

CONCLUSIONS

We postulate, on the basis of the preceding discussion, that the essential bastadin RyR-Ca^{2+} channel pharmacophore may be the hypothetical molecule 2′-hydroxy-2,6-dibromodiphenyl ether (**7**). This is based on a common diphenyl ether substitution pattern found in bastadins from marine sponges of the genus *Ianthella*. The *ortho*-dibromo substituents (*ortho* with respect to the ether oxygen) drives the two phenyl rings to an orthogonal relationship ($\theta_{2-1-O-1'}$ = 180°, ($\theta_{1-O-1'-2'}$ = 92°),[34] which has been shown to increase potency in SAR studies with PCBs.[35,36] The nonplanar diphenyl relationship in bastadins as a feature of RyR1 activity was also noted.[37] In **1a** and **2**, the southern HBDE more closely and consistently attains an orthogonal orientation, whereas the northern HBDE has a larger variance among many of the conformers. The hypothetical molecule 6′-hydroxy-2,2′-dibromodiphenyl ether (**8**), a regioisomer of **7**, may represent a similar or different type of Ca^{2+} modulator in comparison to **7**. Analogues of **8** are commonly found from *Dysidea* marine sponges,[38] as well as being the reported metabolites from polybrominated diphenyl ether flame retardants. In this case the *ortho*-hydroxy-bromo substituents (*ortho* with respect to the ether oxygen) also direct the two phenyl rings toward an orthogonal relationship ($\theta_{2-1-O-1'}$ = 152°, $\theta_{1-O-1'-2'}$ = 106°)[34] but not as close to orthogonal as in **7**. We believe that future SAR and mechanism of action studies with these two different chemotypes are warranted and may reveal the extent to which they mobilize Ca^{2+} via the RyR-Ca^{2+} channel or by a different mechanism of action.[39−41] Such research could be important in understanding the role of BDEs in dysregulation of microsomal Ca^{2+} transport and neurotoxicity.

Our rigorous re-examination of the conformational properties of bastadins that comprise the isobastarane and bastarane-type macrocycle has generated some interesting new insights. We found these macrocycles are flexible and possess a surprising degree of reflection symmetry that generates enantiomeric conformations as exemplified in Figure 3. Overall, the isobastarane conformations for (*E*,*E*)-bastadin 19 (**1a**) are complex, as they can access several distinct ring conformations. In contrast, the bastarane macrocycle in bastadin 5 (**2**) and bastadin 6 (**3**) maintains a similar overall shape. We believe the key to short-term stability of the (*Z*)-oximo amide in **1b** and (*E*,*Z*)-psammaplin A is due to the existence of conformers with intramolecular hydrogen bonds involving the (*Z*)-oxime. Hydrogen bonding impedes oxime isomerization to form the lower energy *E* isomer in solution. Finally, the modeling results provided insights toward understanding the different antiproliferative activity against endothelial cells as well as Ca^{2+} channel modulation activities attributed to bastaranes **2** and **3** versus isobastarane **1a**. A model to explain the differing RyR1-Ca^{2+} channel activities between **1a** versus **2** was proposed that showed both macrocycles could attain a similar overall shape, but constraints of the macrocycle hold the northern 2′-hydroxy-2,3′-dibromophenyl ether (HDBE) in opposite configurations between the macrocycle types. This different configurational position of atoms in **1a** along with the constraints imposed by the macrocycle may not be optimal for binding or channel function.

EXPERIMENTAL SECTION

Modeling Calculations. Molecular modeling was carried out with PCMODEL, version 7.5 (Serena Software). Molecular dynamics was performed with the leapfrog Verlet algorithm. Typical runs were set up with 50,000 time steps (1 fs per time step), sample temperature 300 K, bath temperature 300 K, 1 fs heat transfer time, and 300 fs equilibration time, and structures were sampled every 50 fs. The set of 1000 sampled structures was minimized with the MMFF94 force field, Steepest Descent, then Newton−Raphson gradient, dielectric constant of 1. The MMFF94 force field was used in the present study because of the better fit of predicted versus experimental bond distances obtained with OMPA in comparison to MMX force field. The dynamics-minimization process was repeated using the lowest energy minimized structure from the previous dynamics run until a consistent set of low-energy structures was obtained. The sampled structures from a dynamics run were viewed in the movie view mode, and the macrocycle was observed to undergo a high degree of conformational mobility within each oximo-*N*-phenethyl-3-phenylpropanamide, and with all subgroups (aryls, methylenes, oxime, amide) undergoing complete rotations within the macrocycle. In addition, the torsion angle driving method using $\theta_{C37-C1-C2-C3}$, $\theta_{N4-C5-C6-C7}$, $\theta_{C18-C20-C21-N22}$, and $\theta_{C23-C24-C25-C26}$ was employed to probe for additional global and local minima.

ASSOCIATED CONTENT

Supporting Information. A figure illustrating the modeling results for (*E*,*Z*)-psammaplin A is provided. This material is available free of charge via the Internet at http://pubs.acs.org.

AUTHOR INFORMATION

Corresponding Author

*Tel: 831-459-2603. Fax: 831-459-2935. E-mail: winman@ucsc.edu; phil@chemistry.ucsc.edu.

ACKNOWLEDGMENT

This research was supported by NIH grant R01-CA047135.

DEDICATION

Dedicated to Dr. Koji Nakanishi of Columbia University for his pioneering work on bioactive natural products.

REFERENCES

(1) Renaudet, O.; Reymond, J. L. *Org. Lett.* **2003**, *5*, 4693–4696.
(2) Nsikabaka, S.; Harb, W.; Ruiz-Lopez, M. F. *THEOCHEM* **2006**, *764*, 161–166.
(3) Aoki, H.; Sakai, H.; Kohsaka, M.; Konomi, T.; Hosoda, J.; Kubochi, Y.; Iguchi, E.; Imanaka, H. *J. Antibiot.* **1976**, *29*, 492–500.
(4) Kurita, M.; Jomon, K.; Komori, T.; Miyairi, N.; Aoki, H.; Kuge, S.; Kamiya, T.; Imanaka, H. *J. Antibiot.* **1976**, *29*, 1243–1245.
(5) Quinoa, E.; Crews, P. *Tetrahedron Lett.* **1987**, *28*, 3229–3232.
(6) Arabshahi, L.; Schmitz, F. J. *J. Org. Chem.* **1987**, *52*, 3584–3586.
(7) Jimenez, C.; Crews, P. *Tetrahedron* **1991**, *47*, 2097–2102.
(8) Yagi, H.; Matsunaga, S.; Fusetani, N. *Tetrahedron* **1993**, *49*, 3749–3754.
(9) Cimino, G.; Stefano, S. D.; Minale, L. *Experientia* **1975**, *31*, 756–757.
(10) Motohashi, K.; Gyobu, Y.; Takagi, M.; Shin-ya, K. *J. Antibiot.* **2009**, *62*, 703–704.
(11) Ingavat, N.; Dobereiner, J.; Wiyakrutta, S.; Mahidol, C.; Ruchirawat, S.; Kittakoop, P. *J. Nat. Prod.* **2009**, *72*, 2049–2052.
(12) Calcul, L.; Inman, W. D.; Morris, A. A.; Tenney, K.; Ratnam, J.; McKerrow, J. H.; Valeriote, F. A.; Crews, P. *J. Nat. Prod.* **2010**, *73*, 365–372.
(13) Kelly, W. L.; Townsend, C. A. *J. Am. Chem. Soc.* **2002**, *124*, 8186–8187.
(14) Kelly, W. L.; Townsend, C. A. *J. Bacteriol.* **2005**, *187*, 739–746.
(15) Aoki, S.; Cho, S.; Hiramatsu, A.; Kotoku, N.; Kobayashi, M. *J. Nat. Med.* **2006**, *60*, 231–235.

(16) Kotoku, N.; Hiramatsu, A.; Tsujita, H.; Hirakawa, Y.; Sanagawa, M.; Aoki, S.; Kobayashi, M. *Arch. Pharm. Chem. Life Sci.* **2008**, *341*, 568–577.
(17) Masuno, M. N.; Molinski, T. F. *J. Nat. Prod.* **2003**, *66*, 112–114.
(18) Shorter than normal bond distances were obtained with the MMX force field with the hydrogen bond term for *s-trans*-(*Z*)-OMPA. The N−O bond distance between amide N and oxime O was 2.54 Å; the hydrogen bond distance between amide NH---O oxime was 1.72 Å.
(19) Wei, Y. M., A. E. In *Modeling NMR Chemicals Shifts: Gaining Insights into Structure and Environment*; Facelli, J. C., de Dios, A. C., Eds.; ACS Symposium Series 732; 1999; Chapter 13, pp 177−193.
(20) Hashimoto, M.; Komori, T.; Kamiya, T. *J. Am. Chem. Soc.* **1976**, *98*, 3023–3025.
(21) Molecular mechanics calculations were performed with (*Z*)-2-(oximo)-*N*-isopropyl-2-phenylacetamide (the same model compound used to define the oxime configuration in nocardicins A and B; see ref 20). The calculated bond distances for N−O and the hydrogen bond from oxime O to amide H were 2.83 and 2.37 Å, respectively. The dihedral angle corresponding to $\theta_{N1-C2-C3-C4}$ in OMPA was 117°.
(22) Masuno, M. N.; Hoepker, A. C.; Pessah, I. N.; Molinski, T. F. *Mar. Drugs* **2004**, *2*, 176–184.
(23) Taylor, R.; Kennard, O. *Acc. Chem. Res.* **1984**, *17*, 320–326.
(24) Lommerse, J. P. M.; Price, S. L.; Taylor, R. *J. Comput. Chem.* **1997**, *18*, 757–774.
(25) Molecular mechanics calculations were performed with (*E*)- and (*Z*)-2-(oximo)-*N*-isopropyl-2-phenylacetamide, the same model compounds used to define the oxime configuration in nocardicins A and B; see ref 17. The *Z* isomer was predicted to be lower energy, the relative energy difference being 10.5 kJ/mol. We attribute the lower energy of the *Z* isomer to resonance stablization by the alpha-phenyl, which is coplanar in the *Z* isomer, whereas in the *E* isomer, the phenyl group must twist approximately 50° out of plane due to steric interactions with the (*E*)-oxime.
(26) Approximately only 2−4% of the higher energy conformer would exist at 298 K based on the 10−8 kJ/mol energy difference between conformers.
(27) Kazlauskas, R.; Lidgard, R. O.; Murphy, P. T.; Wells, R. J.; Blount, J. F. *Aust. J. Chem.* **1981**, *34*, 765–786.
(28) Demarco, A.; Llinas, M.; Wuthrich, K. *Biopolymers* **1978**, *17*, 637–650.
(29) Masuno, M. N.; Pessah, I. N.; Olmstead, M. M.; Molinski, T. F. *J. Med. Chem.* **2006**, *49*, 4497–4511.
(30) Zieminska, E.; Lazarewicz, J. W.; Couladouros, E. A.; Moutsos, V. I.; Pitsinos, E. N. *Bioorg. Med. Chem. Lett.* **2008**, *18*, 5734–5737.
(31) Dingemans, M. M. L.; Heusinkveld, H. J.; Bergman, A.; van den Berg, M.; Westerink, R. H. S. *Environ. Health Perspect.* **2010**, *118*, 519–525.
(32) Dingemans, M. M. L.; de Groot, A.; van Kleef, R. G. D. M.; Bergman, A.; van den Berg, M.; Vijverberg, H. P. M.; Westerink, R. H. S. *Environ. Health Perspect.* **2008**, *116*, 637–643.
(33) Suyama, T. L.; Cao, Z. Y.; Murray, T. F.; Gerwick, W. H. *Toxicon* **2010**, *55*, 204–210.
(34) Dihedral angles were measured from the energy-minimized structure. A combination of values ± 90° and ± 180° for the pair of dihedrals would represent an orthogonal relationship between the biphenyl rings.
(35) Wong, P. W.; Brackney, W. R.; Pessah, I. N. *J. Biol. Chem.* **1997**, *272*, 15145–15153.
(36) Pessah, I. N.; Hansen, L. G.; Albertson, T. E.; Garner, C. E.; Ta, T. A.; Do, Z.; Kim, K. H.; Wong, P. W. *Chem. Res. Toxicol.* **2006**, *19*, 92–101.
(37) Chen, L.; Molinski, T. F.; Pessah, I. N. *J. Biol. Chem.* **1999**, *274*, 32603–32612.
(38) Fu, X. O.; Schmitz, E. J.; Govindan, M.; Abbas, S. A.; Hanson, K. M.; Horton, P. A.; Crews, P. *J. Nat. Prod.* **1995**, *58*, 1384–1391.
(39) Dingemans, M. M. L.; van den Berg, M.; Bergman, A.; Westerink, R. H. S. *Toxicol. Sci.* **2010**, *114*, 302–309.
(40) Fonnum, F.; Mariussen, E. *J. Neurochem.* **2009**, *111*, 1327–1347.
(41) Kodavanti, P. R. S. *Dose-Response* **2005**, *3*, 273–305.